

RESEARCH ARTICLE | AUGUST 17 2020

## Coupled fine-scale modeling of the wettability effects: Deformation and fracturing

Tsimur Davydzenka  ; Samuel Fagbemi  ; Pejman Tahmasebi  



*Physics of Fluids* 32, 083308 (2020)

<https://doi.org/10.1063/5.0018455>

 CHORUS

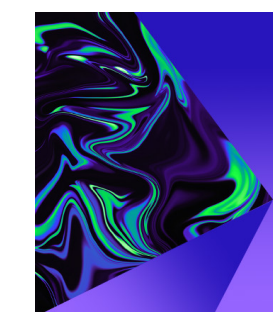


View  
Online



Export  
Citation

CrossMark



## Physics of Fluids

Special Topic:  
Selected Papers from the 2023 Non-Newtonian Fluid Mechanics Symposium in China

**Submit Today**



# Coupled fine-scale modeling of the wettability effects: Deformation and fracturing

Cite as: Phys. Fluids 32, 083308 (2020); doi: 10.1063/5.0018455

Submitted: 16 June 2020 • Accepted: 4 August 2020 •

Published Online: 17 August 2020



View Online



Export Citation



CrossMark

Tsimur Davydzenka,<sup>1</sup> Samuel Fagbemi,<sup>1</sup> and Pejman Tahmasebi<sup>1,2,a)</sup>

## AFFILIATIONS

<sup>1</sup> Department of Petroleum Engineering, University of Wyoming, Laramie, Wyoming 82071, USA

<sup>2</sup> Department of Civil Engineering, University of Wyoming, Laramie, Wyoming 82071, USA

**Note:** This paper is part of the Special Topic on Turbulent and Multiphase Flows.

**a)** Author to whom correspondence should be addressed: ptahmase@uwyo.edu

## ABSTRACT

Multiphase flow in porous media has been thoroughly studied over the years and its importance is encountered in several areas related to geo-materials. One of the most important parameters that control multiphase flow in any complex geometry is wettability, which is an affinity of a given fluid toward a surface. In this paper, we have quantified the effects of wettability on deformation in porous media, along with other parameters that are involved in this phenomenon. To this end, we conducted numerical simulations on a porous medium by coupling the exchanged forces between the fluid and solid. To include the effect of wettability in the medium, we used the Fictitious Domain methodology and coupled it with volume of fluid through which one can model more than one fluid in the system. To observe the effect of wettability on dynamic processes in the designated porous medium, such as deformation, particle–particle contact stresses, particle velocity, and injection pressure, a series of systematic computations were conducted where wettability is varied through five different contact angles. We found that wettability not only controls the fluid propagation patterns but also affects drag forces exerted on the particles during injection such that larger deformations are induced for particles with lower wettability. Our results are also verified against experimental tests.

Published under license by AIP Publishing. <https://doi.org/10.1063/5.0018455>

## I. INTRODUCTION

Flow through porous media is a complex phenomenon that is dependent on various parameters such as fluid composition,<sup>1</sup> morphology of the medium,<sup>2</sup> mineralogy,<sup>3</sup> flow regime,<sup>4</sup> relative permeability,<sup>5–7</sup> and wettability<sup>8</sup> for the case of multiphase flow. These parameters control fluid–fluid and fluid–solid interactions leading to fluid and solid displacements. In this study, we are particularly interested in the effect of wettability on the deformation in porous media. Although the fluid displacement under the influence of wettability has been carefully studied over the years,<sup>8–15</sup> the effect on porous media deformation by fluid affinity to the solid surface still requires much research.

The wettability of a surface is an innate property that affects the interactions between the multiphase fluid and the solid components of a porous medium. More importantly, it is an important determinant factor for the spatial fluid distribution, which subsequently controls the flow and circulation of fluids during dynamic processes.<sup>16</sup>

These interactions lead to two flow regimes, namely drainage (i.e., when the defending fluid is more wetting to the solid than the invading fluid) and imbibition (i.e., when the invading fluid is more wetting to the solid). The properties that are invariably affected by wettability are capillary pressure, relative permeability, rock strength as well as fluid recovery,<sup>17–21</sup> dispersion of tracers, irreducible/residual saturations,<sup>22–25</sup> and electrical properties.<sup>26</sup>

Exploring the effect and importance of wettability in porous media dynamics has led researchers to several defining conclusions. The recent studies on Hele–Shaw cells packed with glass beads<sup>21</sup> have shown that an increase in contact angle stabilizes fluid invasion into a granular pack. Experiments on microfluidic devices patterned with vertical posts also report that the efficiency of displacement increases with the increase of wettability, up to a certain contact angle, after which the trend is reversed.<sup>9</sup> Furthermore, core-flooding studies have shown that the local degree of roughness increases the contact angle and interfacial curvature.<sup>27</sup> However, the inevitable drawback to all experimental setups is that they are

too time demanding and replicating the experiments is problematic. Thus, it is not easy to compare results from different studies.

On the other hand, computational studies have also been conducted for mixed-wet cases.<sup>28</sup> They observed that discontinuous capillary pressures are responsible for sudden changes in the saturation profiles, which in turn leads to significantly different shapes of corresponding saturation paths and demonstrates that the traditional capillary pressure-saturation relationship is not valid under dynamic conditions, as predicted by the theory.<sup>29</sup> Instead, the non-equilibrium capillary theory is required, stating that fluid pressure difference is a function of the time rate of saturation change.<sup>30</sup> Other fairly popular computational methods for simulating multiphase flow in porous media are Smoothed Particles Hydrodynamics (SPH)<sup>31–37</sup> and Lattice Boltzmann (LB).<sup>38–47</sup> Parameters such as fluid viscosity, surface tension, and contact angle in these methods are modeled through interaction forces that are acting between different particles or lattice nodes. However, these methods have been applied mainly for fluid flow problems and are still unproven in terms of their application for coupled fluid-dynamics-solid interaction problems. On the other hand, Volume of Fluid (VOF) is another promising approach for multi-phase flow simulations, which has been effectively implemented to investigate the relation between the half corner angle of pores and the contact angle controlling the temporal evolution of capillary pressure during the invasion of a pore.<sup>48,49</sup>

In flow through porous media, fluids can induce deformation in the solid phase due to the fluid pressure, viscous forces, and wettability conditions, i.e., surface tension forces. Such deformations can be significant under some specific circumstances: deformations in a porous pack during fluid propagation<sup>50–52</sup> or deformation of a soft substrate during droplet movement can vary drastically depending on wettability alone. In order to quantify the deformation, several methods have been introduced to couple fluid flow and solid mechanics. Some of the successful methods are SPH-Finite Element Method (FEM)<sup>53,54</sup> and LBM-Discrete Element Method (DEM),<sup>55–58</sup> which can be used to model granular systems by capturing grain-scale interactions of fluid and solid phases in the system. Modeling of the fluid phase in such methods is achieved by SPH or LBM, which represents the fluids on a discrete lattice mesh while the solid phase is modeled with FEM<sup>59</sup> or DEM.<sup>60</sup> The main advantage of these fluid modeling approaches is that the pore scale fluid dynamics can be modeled more realistically. However, they require a lot of computational power. As a result, they are usually limited to two-dimensional or small cases. Alternatively, computational fluid dynamics (CFD) can be coupled with DEM to model fluid-particle interactions.<sup>61,62</sup> With this technique, the Navier-Stokes (NS) equation governs the fluid dynamics in a meshed geometry and the equations are solved numerically. Moreover, the void fraction, the representative of the presence of solid particles in the mesh, and additional forces are transferred from CFD to DEM, through which the fluid-particle interactions are quantified.<sup>63–75</sup>

A more appealing approach for modeling multiphase flow is DEM-VOF, which is an extension of the CFD-DEM methodology that allows solving more than one fluid in the system. Previous studies have shown that this method is capable of modeling complex three-phase motion and liquid displacement phenomena, which makes DEM-VOF very relevant for our study. Generally, there are two ways in which DEM and VOF can be coupled. In one

scenario, the CFD mesh, which is responsible for solving fluid motion, is larger than the particles (i.e., the unresolved approach),<sup>76–82</sup> and in another scenario, the CFD mesh is considerably smaller than the solid bodies in the system (i.e., resolved immersed-boundary method-VOF)<sup>83–88</sup> or Fictitious Domain methodology (FDM)-VOF.<sup>89,90</sup> Both methods have their own advantages and disadvantages; however, the unresolved method is more appealing at the stage of upscaling the models and reducing computational costs, and the resolved approach is generally more precise than the unresolved one, especially at observing micro-scale phenomena like capillary effects. Since in our study we are interested in observing processes at smaller scales, we adopt the resolved methodology in our simulations.

In this paper, to investigate the effect of wettability on fluid-fluid and fluid-solid interactions, we incorporate VOF into the Fictitious Domain Method<sup>91,92</sup> (FDM) where the solid is modeled through DEM and regard the immiscible phases as a single fluid with different properties. The spatial position of a fluid is described by a color function that carries information about the existing phase and the interface is described as a region with a non-zero color function. By including the solid phase into VOF, we can account for the contact angle, by assigning appropriate boundary conditions to the direction of the color-function gradient at the wall.

The remainder of this paper is organized as follows: In Sec. II, we discuss the methodology that we follow for conducting the simulations, mainly the VOF and FDM equations. Section III focuses on presenting the results obtained for our models. Finally, Sec. IV summarizes this paper.

## II. METHODOLOGY

### A. DEM

In various fluid-solid simulations, inter-particle interactions are often approximated and treated as an averaged lubrication force.<sup>93,94</sup> However, in cases where particles are subject to considerably large displacements (i.e., granular column collapse), particle interactions have to be computed with a greater precision.<sup>95</sup> To this end, the Discrete Element Method (DEM) serves as a well-suited methodology for our simulations.

In classical formulation of DEM, a small overlap between the contacting objects is allowed through the representation of individual particles as “rigid bodies” with “soft” contacts. It is through these small overlaps (usually not larger than 5% of particle radius) that the contact forces are calculated. In calculating forces in particle-particle and particle-wall interactions, a choice of the contact force model plays a significant role. In this study, we adopt the Hertzian force model that neglects cohesive forces between the particles.<sup>96</sup> Here, the governing equations of particle motion are described by the following equations:

$$m_i \frac{d\mathbf{v}_i}{dt} = \sum_{j=1}^{n_i^c} \mathbf{F}_{ij}^c + \mathbf{F}_i^f + m_i \mathbf{g}, \quad (1)$$

$$I_i \frac{d\omega_i}{dt} = \sum_{j=1}^{n_i^c} \mathbf{M}_{ij}^c, \quad (2)$$

where  $\mathbf{v}_i$  is the velocity of particles,  $\mathbf{F}_{ij}^c$  is the contact force on particle  $i$  by particle  $j$  or walls,  $\mathbf{F}_i^f$  is the particle-fluid interaction force

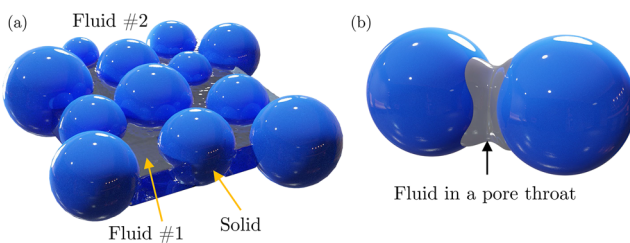


**FIG. 1.** (a) Demonstration of the schematic 3-phase system as used in this study. (b) A closer look at a case wherein the wetting phase to the solid is shown.

acting on particle  $i$ ,  $\mathbf{g}$  is the gravitational acceleration,  $\omega_i$  is the particle angular velocity,  $I_i$  is the moment of inertia, and  $\mathbf{M}_{ij}$  is the moment acting on particle  $i$  by particle  $j$  or walls. As mentioned earlier, we applied Hertzian contact force along with Coulomb's friction law in this paper for describing the interaction between particles (i.e.,  $\mathbf{F}_{ij}^c$ ). Such a multiphysics model is shown in Fig. 1 graphically.

## B. Governing equations

To study the effect of particles on fluid, a new force term to the Navier–Stokes (NS) equations, which takes into consideration the presence of the solid particles, is added to the total force. Thus, we expand upon the works of Glowinski *et al.*<sup>97,98</sup> wherein they have introduced the Fictitious Domain Method. This method is based on Distributed Lagrange Multipliers (DLM). The original method, however, has a limitation, which makes it inefficient due to the need to calculate Lagrangian multipliers explicitly. It was later improved by adding a body force to the NS equations and hence making it no longer necessary to compute the Lagrangian Multiplier explicitly.<sup>99–101</sup> In this study, we follow the method proposed by Hager *et al.*<sup>91</sup> Their method, however, was used to only develop single-phase flow while we extended the work for multiphase flow.

For incompressible multiphase flows, the NS equations can be expressed as a single equation for computing the velocity and pressure fields within the entire domain. The momentum and mass conservation equations for incompressible, Newtonian, and multiphase fluid flow are as follows:

$$\nabla \cdot \mathbf{u} = 0, \quad (3)$$

$$\rho \frac{\partial \hat{\mathbf{u}}}{\partial t} + \nabla \cdot (\rho \hat{\mathbf{u}} \hat{\mathbf{u}}) = -\nabla p + \mu \Delta \hat{\mathbf{u}} + \rho \mathbf{g} + \mathbf{f}_\sigma, \quad (4)$$

where  $\mathbf{g}$  is the gravitational acceleration. The effect of surface tension is accounted for by a local volumetric surface tension force  $\mathbf{f}_\sigma$ . Local averaged density  $\rho$  and viscosity  $\mu$  are a function of distribution of the fluid in local cells and, therefore, are calculated through the local fluid fraction  $\varepsilon$  of the fluid phases. The surface tension force that is included in the NS equations is relevant only in the vicinity of the interface. Advection of volume fraction  $\varepsilon$  is found using

$$\frac{\partial \varepsilon}{\partial t} + \nabla \cdot (\varepsilon \mathbf{u}) = 0. \quad (5)$$

Here,  $\mathbf{u}$  is the local fluid velocity of the interface. Furthermore, local averaged density  $\rho$  and viscosity  $\mu$  are evaluated by linear averaging

of the existing fluids No. 1 ( $\varepsilon = 1$ ) and No. 2 ( $\varepsilon = 0$ ),

$$\rho(\mathbf{x}) = \rho_1 \varepsilon + \rho_2 (1 - \varepsilon), \quad (6)$$

$$\mu(\mathbf{x}) = \mu_1 \varepsilon + \mu_2 (1 - \varepsilon). \quad (7)$$

## C. VOF

In this work, the capillary force is solved using the continuum surface force model (CSF),<sup>102</sup> which is defined by

$$\mathbf{f}_\sigma = \sigma \mathbf{n}, \quad (8)$$

where  $\sigma$  is the surface tension and  $\mathbf{n}$  is the normal to the interface, and is described by

$$\mathbf{n} = -\frac{\nabla \varepsilon}{|\nabla \varepsilon|}. \quad (9)$$

The curvature of the fluid–fluid interface  $\kappa$  is defined by

$$\kappa = \nabla \cdot \mathbf{n}. \quad (10)$$

Furthermore, considering the wall adhesion effect, the contact angle between the solid surface and the fluid can be adopted to modify the unit normal  $\tilde{\mathbf{n}}$  of the phase interface near the surface,

$$\tilde{\mathbf{n}} = \tilde{\mathbf{n}}_w \cos \theta_w + \tilde{\mathbf{t}}_w \sin \theta_w, \quad (11)$$

where  $\tilde{\mathbf{n}}_w$  is the unit vectors normal to the wall,  $\tilde{\mathbf{t}}_w$  is the tangential to the wall, and  $\theta_w$  is the contact angle.

## D. Fictitious domain method

As discussed previously, the main objective of employing the Fictitious Domain Method (FDM) is to perform a correction of the velocity field of the fluid. This can be thought of as adding an additional force term to the NS equations to account for the presence of solid bodies. This approach provides accurate results for moderate Reynolds numbers.

In FDM, once the data from DEM has been processed, the method consists of the following steps:

- 1 Update fluid cell conditions using Eq. (5)
- 2 Evaluation of an interim velocity field  $\hat{\mathbf{u}}$  and related pressure field is as follows:

$$\rho \frac{\partial \hat{\mathbf{u}}}{\partial t} + \nabla \cdot (\rho \hat{\mathbf{u}} \hat{\mathbf{u}}) = -\nabla p + \mu \Delta \hat{\mathbf{u}} + \rho \mathbf{g} + \mathbf{f}_\sigma. \quad (12)$$

This step is achieved through a PISO routine<sup>103,104</sup> (algorithm for solving NS equations numerically).

- 3 Particle tracking: locate cells occupied by each particle.
- 4 Creation of a new velocity field,  $\tilde{\mathbf{u}}$ . To this end, the interim velocity  $\hat{\mathbf{u}}$  is corrected where particles are present by imposing particles' velocity provided by DEM calculations, resulting in new velocity field  $\tilde{\mathbf{u}}$ . This procedure is equivalent to adding a force term  $\mathbf{f}_b$  to the NS equations, where

$$\mathbf{f}_b = \rho \frac{\partial}{\partial t} (\tilde{\mathbf{u}} - \hat{\mathbf{u}}) \quad (13)$$

- 5 The new velocity field  $\tilde{\mathbf{u}}$  is not divergence-free, therefore, a corrected field  $\bar{\mathbf{u}}$  is introduced as

$$\bar{\mathbf{u}} = \tilde{\mathbf{u}} - \nabla \varphi, \quad (14)$$

where  $\varphi$  is a correction factor and  $\tilde{\mathbf{u}}$  is forced to satisfy the divergence-free condition.

Therefore, applying the divergence operator to (14), we obtain a Poisson equation for  $\varphi$ ,

$$\nabla \varphi = \nabla \cdot \tilde{\mathbf{u}} \quad (15)$$

- 6 Correction of the pressure field: after solving Eq. (15), the obtained pressure from the second step is corrected and expanded by the term  $\frac{\partial \varphi}{\partial t}$  as follows:<sup>99,105</sup>

$$\rho \frac{\partial \tilde{\mathbf{u}}}{\partial t} + \nabla \cdot (\rho \tilde{\mathbf{u}} \tilde{\mathbf{u}}) = - \left( \nabla p + \rho \frac{\partial \nabla \varphi}{\partial t} \right) + \mu \Delta \tilde{\mathbf{u}} + \rho g + f_a + f_b. \quad (16)$$

### III. RESULTS AND DISCUSSIONS

To model the effect of wettability on deformation, we used a semi-2D cylindrical pack with 240 spherical particles having the following properties: density = 25 000 kg/m<sup>3</sup>, diameter = 2.5 mm, Young's modulus =  $5 \times 10^6$  Pa, Poisson's ratio = 0.45, restriction coefficient = 0.3, and friction coefficient = 0.1. The solid model is

shown in Fig. 2(a). The pack size was chosen to be 1 mm high and 10 cm in diameter. The simulation domain was initially saturated with silicon oil (receding phase) and water (invading phase) in the center of the domain prior to the actual injection. We used OpenFOAM (for meshing and fluid simulation) and LIGGGHTS (for modeling the disk-shaped particles). The numerical experiments were conducted until the injected phase reached the outer boundaries of the domain. The fluid was injected from the center of the pack with the rate  $Q = 3$  ml/min. A plane at the bottom placed in the center of the domain was used as the inlet while the fluid patches in the radial direction were designated as the outlet.

In this paper, we studied the effect of wettability for both pure fluid and coupled fluid–solid scenarios. In the former case, the particles are not allowed to move, but the particles can move in the latter case by coupling the forces exerted on particles from the fluid motion while the wettability effect is considered. To find a compromise between a very small and a substantial movement of the particles in the pack, we varied the density of the particles and found 25 000 kg/m<sup>3</sup> to be a proper choice in our case. In Table I, we have listed the fluid properties used for the CFD part of the simulations. Each wettability condition was assigned to the walls and solid

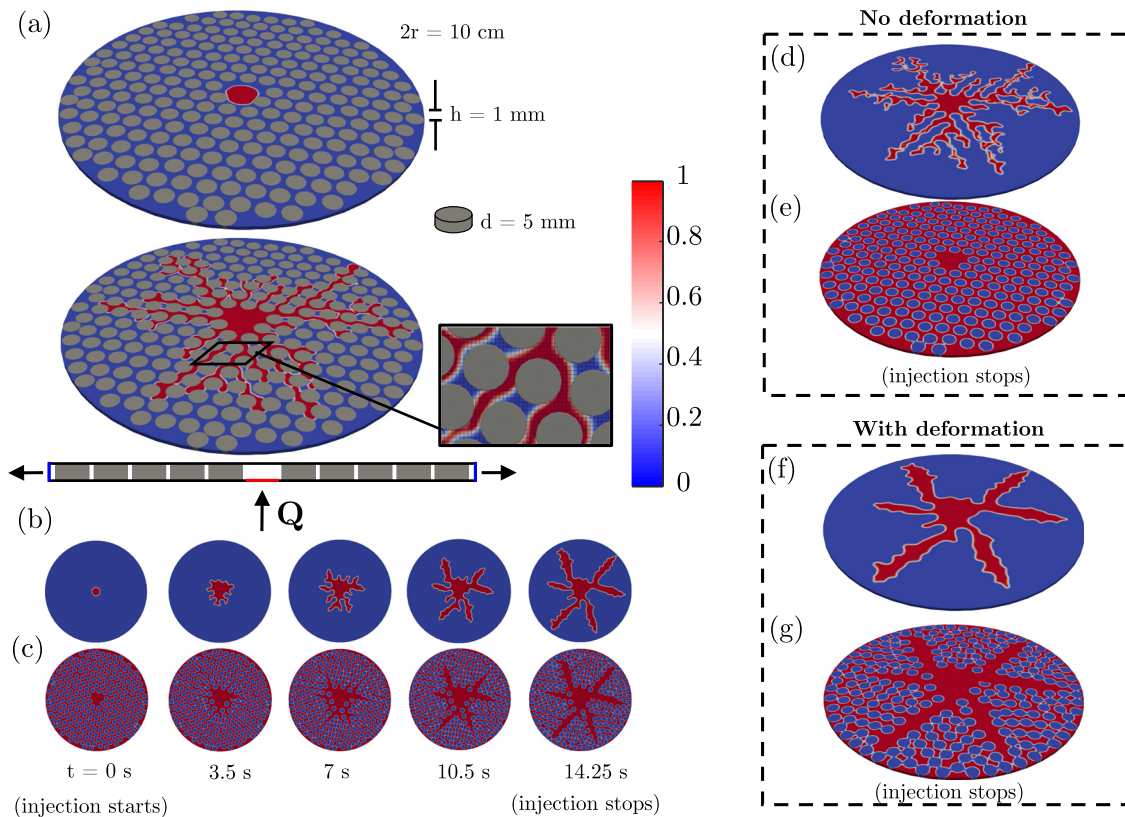


**FIG. 2.** Demonstration of the computational domain (a) with solid particles and resolved CFD mesh represented as wireframe on the left side (for a better particle visibility) and as the surface with edges on the right. An example of  $\theta = 120^\circ$  is presented in (b) and (c) with snapshots of volume fraction for the injected fluid, corresponding to  $t = 0$  s, 3.5 s, 7 s, 10.5 s, and 14.25 s. Volume fraction [(d) and (f)] and void fraction [(e) and (g)] snapshots for the last time step of the simulations with and without deformation, respectively, are presented on the right side of the figure. A color bar in the center of the figure is applicable for parts (a) initial volume fraction in the center of the domain [(b)–(d)].

**TABLE I.** Properties of the fluid used in the simulations.

Property	Value(s)
Contact angle, $\theta$ ( $^{\circ}$ )	{30, 60, 90, 120, 150}
Surface tension, $\sigma$ ( $\text{kg s}^{-2}$ )	0.013
Viscosity of the invading phase, $\nu_i$ ( $\text{m}^2 \text{s}^{-1}$ )	$1 \times 10^{-6}$
Viscosity of the residing phase, $\nu_r$ ( $\text{m}^2 \text{s}^{-1}$ )	$3.54 \times 10^{-4}$
Density of the invading phase, $\rho_i$ ( $\text{kg m}^{-3}$ )	1000
Density of the residing phase, $\rho_r$ ( $\text{kg m}^{-3}$ )	960
Capillary number, $Ca$	4.5

particles through modifying the interface normal Eq. (11), which govern the fluid–solid contact line dynamic. Furthermore, we conducted a sensitivity analysis on the effect of the number of cells for the CFD simulations. Grid independence analysis showed that

the optimal number of cells for our simulation is  $\sim 143\,000$ . For the coupling parameters between CFD and DEM, we used a coupling interval of 1 (meaning that for each DEM time step is immediately coupled with the CFD time step of the same value), with the time step of 0.000 05 for both CFD and DEM parts, and the drag force model was chosen to be Shirgaonkar.<sup>105</sup> Central processing unit (CPU) time for the simulations ranges from 9 h to 12 h per case, depending on how fast the fluid reached the outer boundary.

## A. Results

In this section, we present the results for two-phase fluid interaction with the monodisperse particle domain under five wettability conditions. We validated the results of our method with respect to a well-reviewed experimental study. Furthermore, we quantified the results obtained for cases with and without deformation, compared, and analyzed them. The validation of our results is conducted based on a previous experimental study performed.<sup>9</sup> By creating

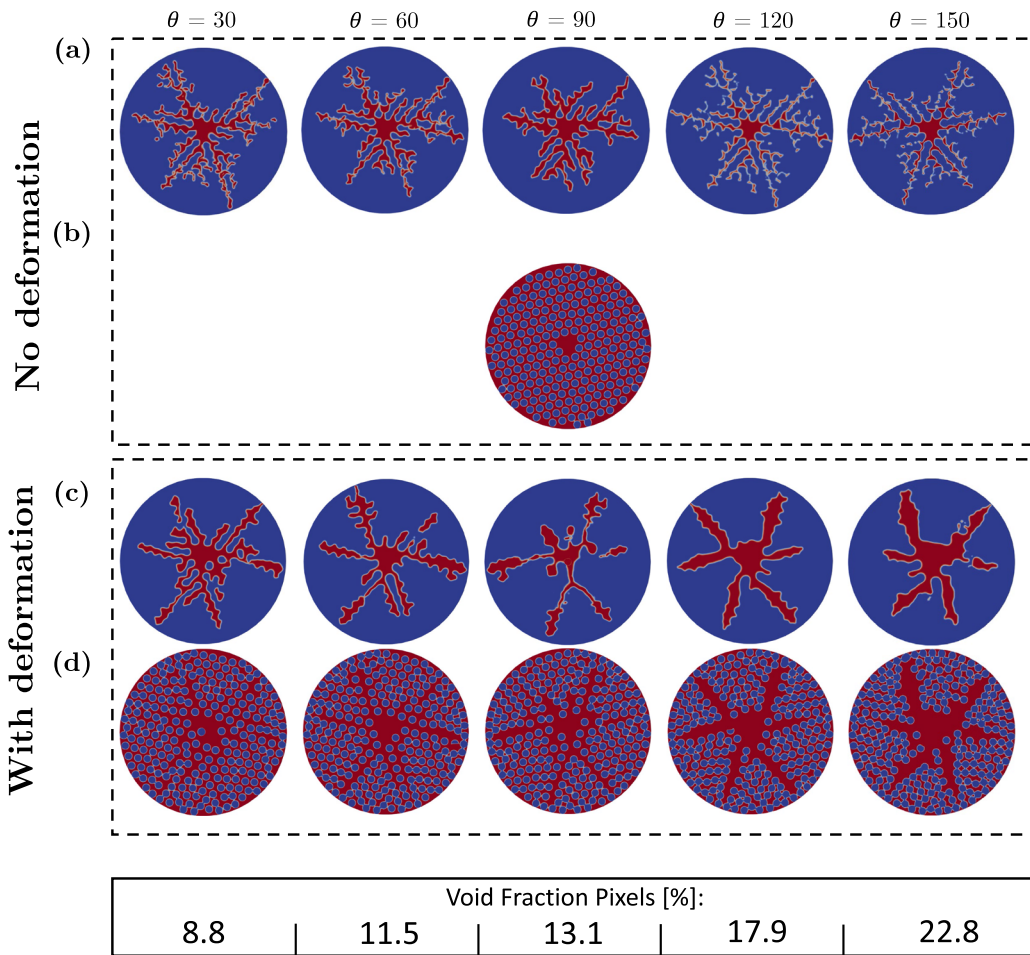


**FIG. 3.** Comparison between cases with and without deformation. The upper part demonstrates the volume fraction (a) and void fraction (b) for the last time step of the simulations, at different contact angles, when particles are fixed throughout the injection. The lower part of the figure represents volume fraction (c) and void fraction (d) for cases, when particle movement is allowed.

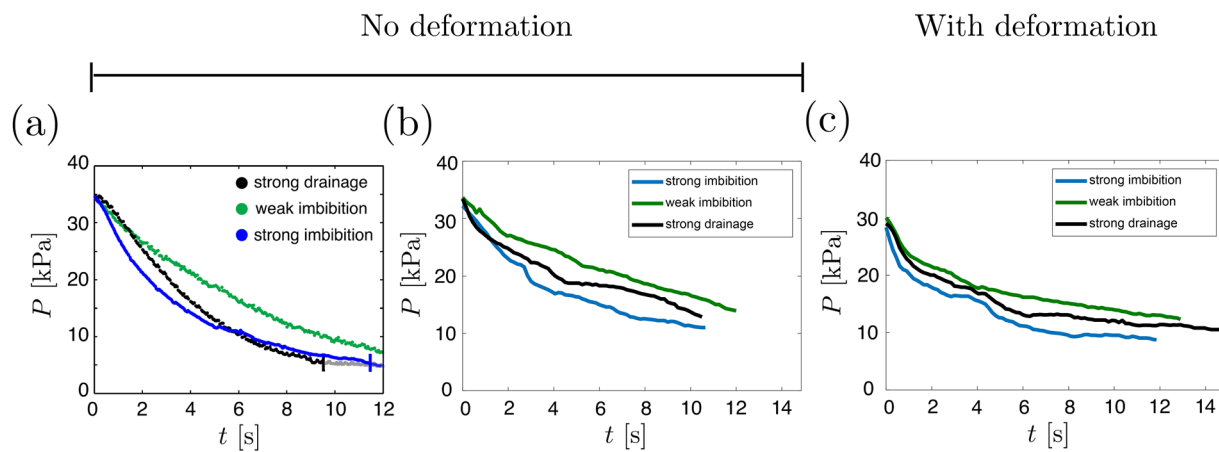


**FIG. 4.** Injection pressure evolution for resolved method cases. (a) Referenced experiments, (b) simulations without deformation, and (c) simulations with deformation.

a similar pack of monodisperse particles, we are able to reproduce the domain and replicate all of the other necessary conditions. We also used adjusted injection rates due to pore volume differences.

The produced pack of particles is shown in Fig. 2. As can be seen, the void space is selected such that it allows particles to move if enough drag force is exerted on them. The simulation is conducted under various wettability conditions, but only one of such cases is graphically shown in Figs. 2(b) and 2(c). The selected pack indicates a continuous distribution of the invading fluid, whereas some degree of fracturing between the particles is also observed. This behavior is more emphasized as the simulation continues. As mentioned, we studied the behavior of fluid under two scenarios, which allows us to better demonstrate how the coupling can affect the fluid and solid responses. Two of such models are provided in Figs. 2(d)–2(g).

Visually speaking, the coupled model represents a more continuous and thicker opening, while the fixed model manifests connectivities with narrow channels, such as those used in the initial pack. A closer view of the models with and without a deformation is provided in Fig. 3, which captures snapshots of the last time step of the simulations. For the cases of coupled modeling [Figs. 3(c) and 3(d)], the void fraction increases along with fluid injection, which indicates fluid force and jamming of particles. As a function of wettability, there is a clear visual trend in the coupled cases, suggesting that the more non-wet the pack becomes, the more deformation is observed. Quantified deformation in the pack, depending on the wettability, is presented in the lower part of this figure as a percentage of the red pixels that constitute a fracture in the pack and confirms the visual trend stated previously. We also incorporated results for injection pressure evolution based on which a direct comparison can be made.

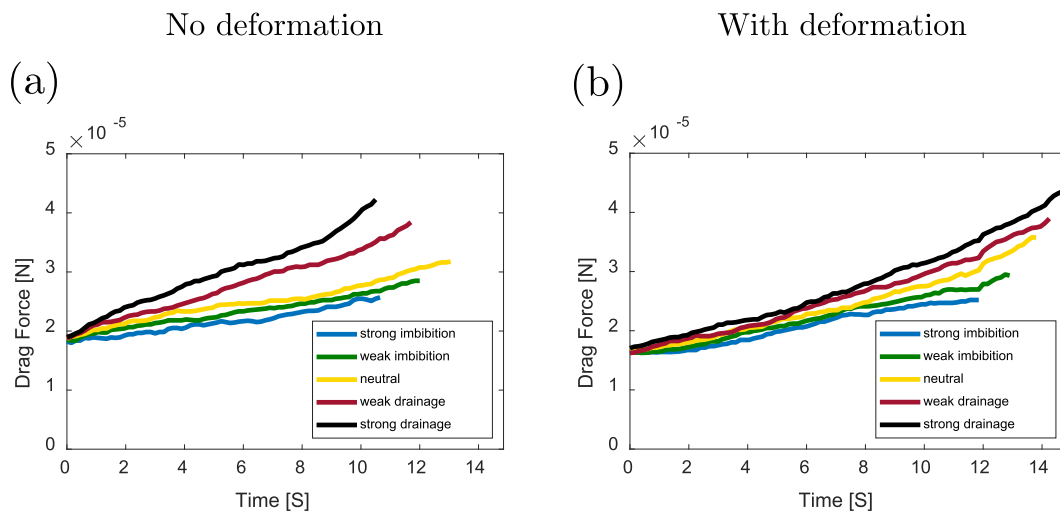


**FIG. 5.** Average drag force in the pack. (a) Cases without deformation and (b) cases with deformation.

The results are shown in Fig. 4. Figure 4(a) is obtained by the experimental study referenced earlier, and Fig. 4(b) corresponds to our computational results when no deformation is imposed. One can observe that the general trend of injection pressure evolution is in agreement with the experiments and considerably close to the experimental data. Furthermore, the results on the effect of wettability in a coupled environment are presented in Fig. 4(c), wherein the particles are allowed to be displaced. As can be observed, the injection pressure in the very first-time step of the simulation is 10%–25% smaller than the non-deformed (fixed) models. This considerable pressure drop is related to the fact that, as particles are allowed to move in the domain, the injected fluid is no longer forced to propagate in initially small channels between the particles, rather it opens up new apertures by displacing the particles. Therefore, as injecting proceeds, the channels, which were previously narrow, make larger channels due to the displacement of the particles. However, at the same time, the pressure difference between cases with and without deformation becomes less noticeable, as the pack becomes more and more packed as the particles are not allowed to leave the domain. We also observe that, for all of the cases with different wettability conditions, the injection pressure is no longer receding or dropping at a high rate at final stages of simulation, which is in accordance with the fact that the pack becomes jammed at its outer boundaries by the end of the simulation and, thus, pressure has to build up before the fluid can propagate.

To further quantify the effect of wettability and capillary number on deformation, as well as quantify the size of possible openings/fractures created by the injected fluid, we used a pixel count method to count the red pixels in void fraction data; see Fig. 2(g). The pixel count shows that the highest deformation in the pack occurred when the injected fluid is at its greatest non-wetting state, implying that lesser contact angles resulted in lesser deformation. These observations are consistent with a similar study exploring the effect of wettability on deformation by means of coupling pore network models with DEM.<sup>51</sup>

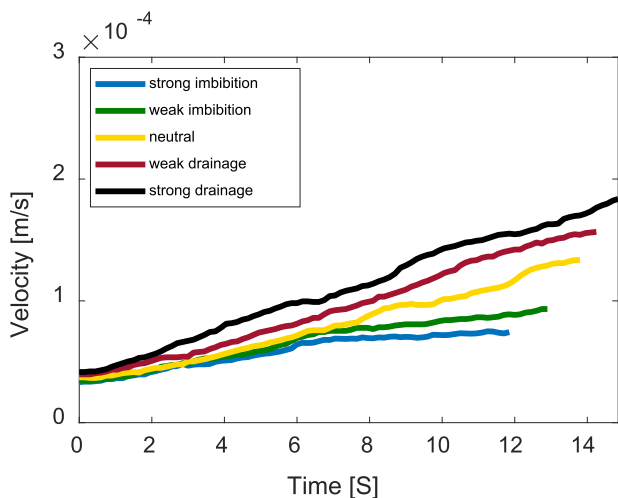


FIG. 6. Evolution of average particle velocity in the pack throughout the deformation case simulation.

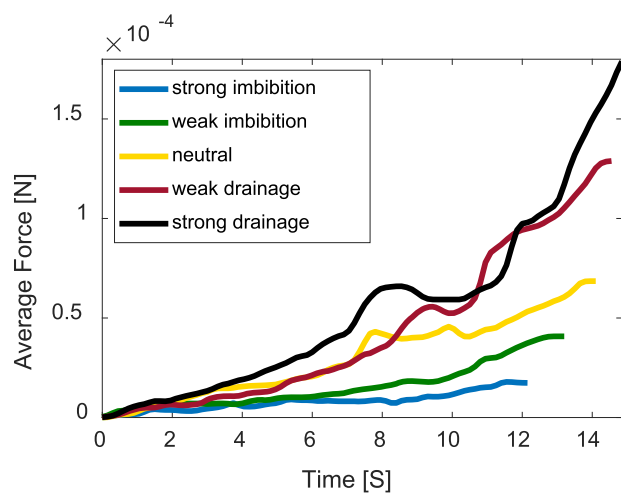


FIG. 7. Evolution of average normal contact force magnitude in the pack for different wettability conditions.

To further quantify the effects of deformation, we included the average drag force and particle velocity in Figs. 5 and 6, respectively. It can be seen from the results that reducing the wettability results in higher values of average drag force in the pack, and higher values of average particle velocity for all cases. These observations are consistent with the deformation observed and quantified in the pack.

Finally, we quantified the average normal contact forces (Fig. 7) and average particle dislocation (Fig. 8) in the pack for all of the deformation cases. We observe that the trends are consistent with the drag force evolution and the total deformation in the pack (found by the pixel count procedure). It can be noted that for all wettability conditions, since the initial stages of the simulation had particles being barely in contact with each other, the values of average contact

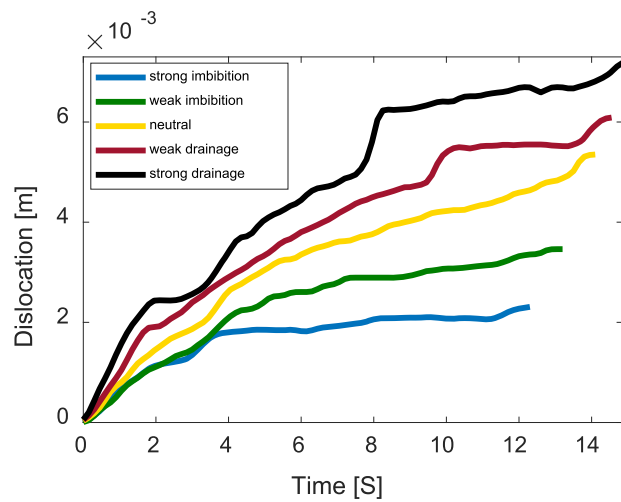


FIG. 8. Evolution of average particle dislocation in the pack throughout for different wettability conditions.

forces are relatively insignificant. However, toward the end of fluid propagation in the pack, these values become considerably higher and increase at a higher rate since the pack becomes more and more jammed. Furthermore, as can be seen in Fig. 8, the average dislocation of the particles in the pack increases considerably faster at the initial stages of the simulation than at the end, which indicates that at the early phase of the simulation, the pack is loose and the jamming forces between the particles (Fig. 7) are not high. Nonetheless, the average dislocation for all wettability conditions becomes less significant toward the final stages of the simulation, where the pack becomes jammed, at which point, the forces in the pack generated by fluid propagation is converted into higher contact forces between the particles.

#### IV. CONCLUSIONS

The aim of this paper was to present the capability of a novel FDM-VOF methodology to numerically solve multiphase flow through porous media. We implemented the Fictitious Domain Method (FDM) in order to represent solid particles in a resolved manner on a non-body conformal Cartesian CFD grid. Volume of Fluid (VOF), a sharp interface and mass conservative method, was used to track the fluid–fluid interface, and the continuum surface force (CSF) model was used to numerically solve the volumetric surface tension force. The choice of the CSF model in our method is justified due to its simplicity and precision, when dealing with complex solid boundaries. The methodology was validated by comparing numerical results of injection pressure evolution with experiments in microfluidic cells.

To observe the capability of the solver and study the effect of wettability on dynamic processes in the porous 2D system, five contact angles, representing the wettability conditions, were applied to the walls and particles in the medium. As a result of this study, the following observations were obtained:

1. The observed trend of deformation in the pack demonstrated that the higher the contact angle of the particles and walls of the pack, the higher the drag forces and hence, more deformation induced in the solid domain. Thus, greater contact forces were observed, which are consistent with previous numerical studies.
2. For all wettability conditions, the observed trend of the fluid displacement pattern indicated that, at high contact angles, the pack gets invaded more easily, which is confirmed and validated by the results of injection pressure evolution.

In the future, these models can be extended to simulate more complex 3D problems.

#### ACKNOWLEDGMENTS

This study was partially supported by the NSF (Grant No. CMMI-2000966), NIH (Grant No. P20GM103432), and NASA (Grant No. 80NSSC19M0061).

#### NOMENCLATURE

$f_b$	body force
$f_\sigma$	surface force term
$F_{ij}^c$	contact force on particles

$F_i^f$	particle–fluid interaction force, acting on particle $i$
$I_i$	moment of inertia
$M_{ij}^c$	moment, acting on particle $i$ by particle $j$ or walls
$\mathbf{n}$	interface normal vector
$\mathbf{n}_w$	unit vector normal to the wall
$p$	fluid pressure
$\mathbf{t}_w$	unit vector tangential to the wall
$\mathbf{u}$	fluid velocity
$\bar{\mathbf{u}}$	corrected velocity field
$\tilde{\mathbf{u}}$	velocity field given by adding a body force term in NS eqs
$\hat{\mathbf{u}}$	interim velocity field
$v_i$	particle velocity
$\varepsilon$	local fluid fraction
$\theta_w$	contact angle
$\kappa$	fluid interface curvature
$\mu$	dynamic viscosity
$\rho$	fluid density
$\sigma$	surface tension
$\varphi$	correction factor
$\omega_i$	angular velocity

#### DATA AVAILABILITY

The data that support the findings of this study are available from the corresponding author upon reasonable request.

#### REFERENCES

1. S. Abaci, J. S. Edwards, and B. N. Whittaker, “Relative permeability measurements for two phase flow in unconsolidated sands,” *Mine Water Environ.* **11**, 11 (1992).
2. J. Hommel, E. Coltman, and H. Class, “Porosity–permeability relations for evolving pore space: A review with a focus on (bio-)geochemically altered porous media,” *Transp. Porous Media* **124**, 589 (2018).
3. I. Aksu, E. Bazilevskaya, and Z. T. Karpyn, “Swelling of clay minerals in unconsolidated porous media and its impact on permeability,” *GeoResj* **7**, 1 (2015).
4. W. A. Moseley and V. K. Dhir, “Capillary pressure-saturation relations in porous media including the effect of wettability,” *J. Hydrol.* **178**, 33 (1996).
5. R. Hu, Y. Chen, H. Liu, and C. Zhou, “A relative permeability model for deformable soils and its impact on coupled unsaturated flow and elasto-plastic deformation processes,” *Sci. China Technol. Sci.* **58**, 1971 (2015).
6. R. Lenormand, C. Zarcone, and A. Sarr, “Mechanisms of the displacement of one fluid by another in a network of capillary ducts,” *J. Fluid Mech.* **135**, 337 (1983).
7. R. Lenormand, E. Touboul, and C. Zarcone, “Numerical models and experiments on immiscible displacements in porous media,” *J. Fluid Mech.* **189**, 165 (1988).
8. J. Zhao, Q. Kang, J. Yao, H. Viswanathan, R. Pawar, L. Zhang, and H. Sun, “The effect of wettability heterogeneity on relative permeability of two-phase flow in porous media: A lattice Boltzmann study,” *Water Resour. Res.* **54**, 1295, <https://doi.org/10.1002/2017wr021443> (2018).
9. B. Zhao, C. W. MacMinn, and R. Juanes, “Wettability control on multiphase flow in patterned microfluidics,” *Proc. Natl. Acad. Sci. U. S. A.* **113**, 10251 (2016).
10. C.-X. Zhao, “Multiphase flow microfluidics for the production of single or multiple emulsions for drug delivery,” *Adv. Drug Delivery Rev.* **65**, 1420 (2013).
11. R. Holtzman, “Effects of pore-scale disorder on fluid displacement in partially-wettable porous media,” *Sci. Rep.* **6**, 36221 (2016).
12. Y. Qi, X. Luo, Y. Wang, N. Liu, B. Zhou, J. Yan, and L. Zhang, “Mechanical study of the effect of fractional-wettability on multiphase fluid flow,” *Int. J. Multiphase Flow* **93**, 205 (2017).
13. S. A. Bradford, L. M. Abriola, and F. J. Leij, “Wettability effects on two- and three-fluid relative permeabilities,” *J. Contam. Hydrol.* **28**, 171 (1997).

- <sup>14</sup>M.-H. Hui and M. J. Blunt, "Effects of wettability on three-phase flow in porous media," *J. Phys. Chem. B* **104**, 3833 (2000).
- <sup>15</sup>D. M. O'Carroll, K. G. Mumford, L. M. Abriola, and J. I. Gerhard, "Influence of wettability variations on dynamic effects in capillary pressure," *Water Resour. Res.* **46**, W08505, <https://doi.org/10.1029/2009wr008712> (2010).
- <sup>16</sup>C. McPhee, J. Reed, and I. Zubizarreta, *Core Analysis: A Best Practice Guide* (Elsevier, 2015).
- <sup>17</sup>P. Chen and K. Mohanty, "Surfactant-mediated spontaneous imbibition in carbonate rocks at harsh reservoir conditions," *SPE J.* **18**, 124 (2013).
- <sup>18</sup>N. Morrow and J. Buckley, "Improved oil recovery by low-salinity waterflooding," *J. Pet. Technol.* **63**, 106 (2011).
- <sup>19</sup>D. C. Standnes and T. Austad, "Wettability alteration in chalk," *J. Pet. Sci. Eng.* **28**, 123 (2000).
- <sup>20</sup>D. C. Standnes and T. Austad, "Wettability alteration in carbonates," *Colloids Surf., A* **216**, 243 (2003).
- <sup>21</sup>M. Trojer, M. L. Szulczecki, and R. Juanes, "Stabilizing fluid-fluid displacements in porous media through wettability alteration," *Phys. Rev. Appl.* **3**, 054008 (2015).
- <sup>22</sup>P. P. Jadhunandan and N. R. Morrow, "Effect of wettability on waterflood recovery for crude-oil/brine/rock systems," *SPE Reservoir Eng.* **10**, 40 (1995).
- <sup>23</sup>J. S. Buckley, Y. Liu, and S. Monterleet, "Mechanisms of wetting alteration by crude oils," *SPE J.* **3**, 54 (1998).
- <sup>24</sup>E. J. Manrique, V. E. Muci, and M. E. Gurfinkel, "EOR field experiences in carbonate reservoirs in the United States," *SPE Reservoir Eval. Eng.* **10**, 667 (2007).
- <sup>25</sup>E. J. Spiteri, R. Juanes, M. J. Blunt, and F. M. Orr, "A new model of trapping and relative permeability hysteresis for all wettability characteristics," *SPE J.* **13**, 277 (2008).
- <sup>26</sup>A. L. Ogunberu and M. Ayub, "The role of wettability in petroleum recovery," *Pet. Sci. Technol.* **23**, 169 (2005).
- <sup>27</sup>A. AlRatrou, M. J. Blunt, and B. Bijeljic, "Wettability in complex porous materials, the mixed-wet state, and its relationship to surface roughness," *Proc. Natl. Acad. Sci. U. S. A.* **115**, 8901 (2018).
- <sup>28</sup>P. Tahmasebi and S. Kamrava, "Rapid multiscale modeling of flow in porous media," *Phys. Rev. E* **98**, 052901 (2018).
- <sup>29</sup>R. Holm, M. I. J. van Dijke, and S. Geiger, "Three-phase flow modelling using pore-scale capillary pressures and relative permeabilities for mixed-wet media at the continuum-scale," *Transp. Porous Media* **81**, 423 (2010).
- <sup>30</sup>V. Joekar-Niasar, S. M. Hassanizadeh, and H. K. Dahle, "Non-equilibrium effects in capillarity and interfacial area in two-phase flow: Dynamic pore-network modelling," *J. Fluid Mech.* **655**, 38 (2010).
- <sup>31</sup>A. M. Tartakovsky and P. Meakin, "Pore scale modeling of immiscible and miscible fluid flows using smoothed particle hydrodynamics," *Adv. Water Resour.* **29**, 1464 (2006).
- <sup>32</sup>U. C. Bandara, A. M. Tartakovsky, and B. J. Palmer, "Pore-scale study of capillary trapping mechanism during CO<sub>2</sub> injection in geological formations," *Int. J. Greenhouse Gas Control* **5**, 1566 (2011).
- <sup>33</sup>G. G. Pereira, M. Prakash, and P. W. Cleary, "SPH modelling of fluid at the grain level in a porous medium," *Appl. Math. Model.* **35**, 1666 (2011).
- <sup>34</sup>S. Wu, M. Rubinato, and Q. Gui, "SPH simulation of interior and exterior flow field characteristics of porous media," *Water* **12**, 918 (2020).
- <sup>35</sup>P. Kunz, I. M. Zarikos, N. K. Karadimitriou, M. Huber, U. Nieken, and S. M. Hassanizadeh, "Study of multi-phase flow in porous media: Comparison of SPH simulations with micro-model experiments," *Transp. Porous Media* **114**, 581 (2016).
- <sup>36</sup>J. Ai, J.-F. Chen, J. M. Rotter, and J. Y. Ooi, "Assessment of rolling resistance models in discrete element simulations," *Powder Technol.* **206**, 269 (2011).
- <sup>37</sup>H. Bassar, M. Rudman, and E. Daly, "SPH modelling of multi-fluid lock-exchange over and within porous media," *Adv. Water Resour.* **108**, 15 (2017).
- <sup>38</sup>C. Pan, M. Hilpert, and C. T. Miller, "Lattice-Boltzmann simulation of two-phase flow in porous media," *Water Resour. Res.* **40**, W01501, <https://doi.org/10.1029/2003wr002120> (2004).
- <sup>39</sup>B. Ahrenholz, A. Peters, A. Kaestner, M. Krafczyk, and W. Durner, "Prediction of capillary hysteresis in a porous material using lattice-Boltzmann methods and comparison to experimental data and a morphological pore network model," *Adv. Water Resour.* **31**, 1151 (2008).
- <sup>40</sup>Y. H. Qian, D. D'Humières, and P. Lallemand, "Lattice BGK models for Navier-Stokes equation," *Europhys. Lett.* **17**, 479 (1992).
- <sup>41</sup>S. Chen and G. D. Doolen, "Lattice Boltzmann method for fluid flows," *Annu. Rev. Fluid Mech.* **30**, 329 (1998).
- <sup>42</sup>E. Fattah, C. Waluga, B. Wohlmuth, U. Rüde, M. Manhart, and R. Helmig, "Lattice Boltzmann methods in porous media simulations: From laminar to turbulent flow," *Comput. Fluids* **140**, 247 (2016).
- <sup>43</sup>Q. Kang, P. C. Lichtner, and D. R. Janecky, "Lattice Boltzmann method for reacting flows in porous media," *Adv. Appl. Math. Mech.* **2**, 545 (2010).
- <sup>44</sup>A. Nabovati and A. C. M. Sousa, *New Trends in Fluid Mechanics Research* (Springer Berlin Heidelberg, 2007), pp. 518–521.
- <sup>45</sup>M. A. A. Spaid and F. R. Phelan, "Lattice Boltzmann methods for modeling microscale flow in fibrous porous media," *Phys. Fluids* **9**, 2468 (1997).
- <sup>46</sup>D. M. Freed, "Lattice-Boltzmann method for macroscopic porous media modeling," *Int. J. Mod. Phys. C* **09**, 1491 (1998).
- <sup>47</sup>J. Li and D. Brown, "Upscaled lattice Boltzmann method for simulations of flows in heterogeneous porous media," *Geofluids* **2017**, 1740693 (2013).
- <sup>48</sup>H. S. Rabbani, V. Joekar-Niasar, and N. Shokri, "Effects of intermediate wettability on entry capillary pressure in angular pores," *J. Colloid Interface Sci.* **473**, 34 (2016).
- <sup>49</sup>S. Fagbemi, P. Tahmasebi, and M. Piri, "Numerical modeling of strongly coupled microscale multiphase flow and solid deformation," *Int. J. Numer. Anal. Methods Geomech.* **44**, 161 (2020).
- <sup>50</sup>J. Bueno, Y. Bazilevs, R. Juanes, and H. Gomez, "Droplet motion driven by tensotaxis," *Extreme Mech. Lett.* **13**, 10 (2017).
- <sup>51</sup>Y. Meng, B. K. Primkulov, Z. Yang, C. Y. Kwok, and R. Juanes, "Jamming transition and emergence of fracturing in wet granular media," *Phys. Rev. Res.* **2**, 022012 (2020).
- <sup>52</sup>A. K. Jain and R. Juanes, "Preferential mode of gas invasion in sediments: Grain-scale mechanistic model of coupled multiphase fluid flow and sediment mechanics," *J. Geophys. Res.* **114**, <https://doi.org/10.1029/2008jb006002> (2009).
- <sup>53</sup>H. H. Bui and G. D. Nguyen, "A coupled fluid-solid SPH approach to modelling flow through deformable porous media," *Int. J. Solids Struct.* **125**, 244 (2017).
- <sup>54</sup>P. Truong-Thi, H. Nguyen-Xuan, and M. Abdel Wahab, *Lecture Notes in Civil Engineering* (Springer, 2019), pp. 187–201.
- <sup>55</sup>A. Hassanpour, H. Tan, A. Bayly, P. Gopalkrishnan, B. Ng, and M. Ghadiri, "Analysis of particle motion in a paddle mixer using discrete element method (DEM)," *Powder Technol.* **206**, 189 (2011).
- <sup>56</sup>G. T. Houslsby, "Potential particles: A method for modelling non-circular particles in DEM," *Comput. Geotech.* **36**, 953 (2009).
- <sup>57</sup>C. H. Rycroft, A. V. Orpe, and A. Kudrolli, "Physical test of a particle simulation model in a sheared granular system," *Phys. Rev. E* **80**, 031305 (2009).
- <sup>58</sup>L.-S. Lu and S.-S. Hsiao, "DEM simulation of particle mixing in a sheared granular flow," *Particuology* **6**, 445 (2008).
- <sup>59</sup>A. Hrennikoff, "Solution of problems of elasticity by the frame-work method," *Appl. Sci. Res.* **8**, 619 (1941).
- <sup>60</sup>P. A. Cundall and O. D. L. Strack, "A discrete numerical model for granular assemblies," *Géotechnique* **29**, 47 (1979).
- <sup>61</sup>P. Tahmasebi and S. Kamrava, "A pore-scale mathematical modeling of fluid-particle interactions: Thermo-hydro-mechanical coupling," *Int. J. Greenhouse Gas Control* **83**, 245 (2019).
- <sup>62</sup>X. Zhang and P. Tahmasebi, "Micromechanical evaluation of rock and fluid interactions," *Int. J. Greenhouse Gas Control* **76**, 266 (2018).
- <sup>63</sup>K. W. Chu, B. Wang, A. B. Yu, and A. Vince, "CFD-DEM modelling of multiphase flow in dense medium cyclones," *Powder Technol.* **193**, 235 (2009).
- <sup>64</sup>C. Wu, Y. Cheng, Y. Ding, and Y. Jin, "CFD-DEM simulation of gas-solid reacting flows in fluid catalytic cracking (FCC) process," *Chem. Eng. Sci.* **65**, 542 (2010).
- <sup>65</sup>Y. Zhao, Y. Ding, C. Wu, and Y. Cheng, "Numerical simulation of hydrodynamics in downers using a CFD-DEM coupled approach," *Powder Technol.* **199**, 2 (2010).
- <sup>66</sup>K. Washino, H. S. Tan, M. J. Hounslow, and A. D. Salman, "A new capillary force model implemented in micro-scale CFD-DEM coupling for wet granulation," *Chem. Eng. Sci.* **93**, 197 (2013).

- <sup>67</sup>X. Chen, W. Zhong, X. Zhou, B. Jin, and B. Sun, "CFD-DEM simulation of particle transport and deposition in pulmonary airway," *Powder Technol.* **228**, 309 (2012).
- <sup>68</sup>J. Zhao and T. Shan, "Coupled CFD-DEM simulation of fluid-particle interaction in geomechanics," *Powder Technol.* **239**, 248 (2013).
- <sup>69</sup>Z. B. Tong, B. Zheng, R. Y. Yang, A. B. Yu, and H. K. Chan, "CFD-DEM investigation of the dispersion mechanisms in commercial dry powder inhalers," *Powder Technol.* **240**, 19 (2013).
- <sup>70</sup>H. Li, Y. Li, F. Gao, Z. Zhao, and L. Xu, "CFD-DEM simulation of material motion in air-and-screen cleaning device," *Comput. Electron. Agric.* **88**, 111 (2012).
- <sup>71</sup>C. T. Jayasundara, R. Y. Yang, B. Y. Guo, A. B. Yu, I. Govender, A. Mainza, A. van der Westhuizen, and J. Rubenstein, "CFD-DEM modelling of particle flow in IsaMills—Comparison between simulations and PEPT measurements," *Miner. Eng.* **24**, 181 (2011).
- <sup>72</sup>K. W. Chu, B. Wang, D. L. Xu, Y. X. Chen, and A. B. Yu, "CFD-DEM simulation of the gas-solid flow in a cyclone separator," *Chem. Eng. Sci.* **66**, 834 (2011).
- <sup>73</sup>X. Ku, T. Li, and T. Løvås, "CFD-DEM simulation of biomass gasification with steam in a fluidized bed reactor," *Chem. Eng. Sci.* **122**, 270 (2015).
- <sup>74</sup>M. H. Zhang, K. W. Chu, F. Wei, and A. B. Yu, "A CFD-DEM study of the cluster behavior in riser and downer reactors," *Powder Technol.* **184**, 151 (2008).
- <sup>75</sup>D. Jajcevic, E. Siegmann, C. Radeke, and J. G. Khinast, "Large-scale CFD-DEM simulations of fluidized granular systems," *Chem. Eng. Sci.* **98**, 298 (2013).
- <sup>76</sup>G. Pozzetti and B. Peters, "On the choice of a phase interchange strategy for a multiscale DEM-VOF method," *AIP Conf. Proc.* **1863**, 180002 (2017).
- <sup>77</sup>G. Pozzetti and B. Peters, "A multiscale DEM-VOF method for the simulation of three-phase flows," *Int. J. Multiphase Flow* **99**, 186 (2018).
- <sup>78</sup>L. Li and B. Li, "Implementation and validation of a volume-of-fluid and discrete-element-method combined solver in OpenFOAM," *Particuology* **39**, 109 (2018).
- <sup>79</sup>L. Jing, C. Y. Kwok, Y. F. Leung, and Y. D. Sobral, "Extended CFD-DEM for free-surface flow with multi-size granules," *Int. J. Numer. Anal. Methods Geomech.* **40**, 62 (2016).
- <sup>80</sup>L. Wu, M. Gong, and J. Wang, "Development of a DEM-VOF model for the turbulent free-surface flows with particles and its application to stirred mixing system," *Ind. Eng. Chem. Res.* **57**, 1714 (2018).
- <sup>81</sup>X. Sun and M. Sakai, "Three-dimensional simulation of gas-solid-liquid flows using the DEM-VOF method," *Chem. Eng. Sci.* **134**, 531 (2015).
- <sup>82</sup>S. T. W. Kurunuru, E. Sauret, S. C. Saha, and Y. T. Gu, in Proceedings of the 20th Australasian Fluid Mechanics Conference (AFMC), 2016.
- <sup>83</sup>J. Yang and F. Stern, in 18th AIAA Computational Fluid Dynamics Conference, 2007.
- <sup>84</sup>S. Gsell, T. Bonometti, and D. Astruc, "A coupled volume-of-fluid/immersed-boundary method for the study of propagating waves over complex-shaped bottom: Application to the solitary wave," *Comput. Fluids* **131**, 56 (2016).
- <sup>85</sup>C. Zhang, N. Lin, Y. Tang, and C. Zhao, "A sharp interface immersed boundary/VOF model coupled with wave generating and absorbing options for wave-structure interaction," *Comput. Fluids* **89**, 214 (2014).
- <sup>86</sup>A. O'Brien and M. Bussmann, "A volume-of-fluid ghost-cell immersed boundary method for multiphase flows with contact line dynamics," *Comput. Fluids* **165**, 43 (2018).
- <sup>87</sup>H. V. Patel, S. Das, J. A. M. Kuipers, J. T. Padding, and E. A. J. F. Peters, "A coupled volume of fluid and immersed boundary method for simulating 3D multiphase flows with contact line dynamics in complex geometries," *Chem. Eng. Sci.* **166**, 28 (2017).
- <sup>88</sup>X. Sun and M. Sakai, "Numerical simulation of two-phase flows in complex geometries by using the volume-of-fluid/immersed-boundary method," *Chem. Eng. Sci.* **139**, 221 (2016).
- <sup>89</sup>A. Pathak and M. Raessi, "A three-dimensional volume-of-fluid method for reconstructing and advecting three-material interfaces forming contact lines," *J. Comput. Phys.* **307**, 550 (2016).
- <sup>90</sup>H. R. Mottahedi, M. Anbarsooz, and M. Passandideh-Fard, "Application of a fictitious domain method in numerical simulation of an oscillating wave surge converter," *Renewable Energy* **121**, 133 (2018).
- <sup>91</sup>A. Hager, C. Kloss, S. Pirker, and C. Goniva, in 9th International Conference on CFD in the Minerals and Process Industries, Melbourne, Australia, 2011.
- <sup>92</sup>A. Hager, C. Kloss, S. Pirker, and C. Goniva, "Parallel resolved open source CFD-DEM: Method, validation and application," *J. Comput. Multiphase Flows* **6**, 13 (2014).
- <sup>93</sup>E. J. Hinch and J. M. Serayssol, "The elastohydrodynamic collision of two spheres," *J. Fluid Mech.* **163**, 479 (1986).
- <sup>94</sup>G. C. Yang, L. Jing, C. Y. Kwok, and Y. D. Sobral, "A comprehensive parametric study of LBM-DEM for immersed granular flows," *Comput. Geotech.* **114**, 103100 (2018).
- <sup>95</sup>V. Topin, Y. Monerie, F. Perales, and F. Radjai, *Phys. Rev. Lett.* **109**, 188001 (2012).
- <sup>96</sup>H. Hertz, "Über die Berührung fester elastischer Körper (On the contact of solid elastic bodies)," *J. Pure Appl. Math.* (1881).
- <sup>97</sup>R. Glowinski, T. Pan, T. I. Hesla, D. D. Joseph, and J. Périoux, "A distributed Lagrange multiplier/fictitious domain method for flows around moving rigid bodies: Application to particulate flow," *Int. J. Numer. Methods Fluids* **30**, 1043 (1999).
- <sup>98</sup>R. Glowinski, T. W. Pan, T. I. Hesla, D. D. Joseph, and J. Périoux, "A fictitious domain approach to the direct numerical simulation of incompressible viscous flow past moving rigid bodies: Application to particulate flow," *J. Comput. Phys.* **169**, 363 (2001).
- <sup>99</sup>N. A. Patankar, "A formulation for fast computations of rigid particulate flows," Center for Turbulence Research, Annual Research Briefs (2001), p. 185.
- <sup>100</sup>C. Diaz-Goano, P. D. Minev, and K. Nandakumar, "A fictitious domain/finite element method for particulate flows," *J. Comput. Phys.* **192**, 105 (2003).
- <sup>101</sup>Z. Yu and X. Shao, "A direct-forcing fictitious domain method for particulate flows," *J. Comput. Phys.* **227**, 292 (2007).
- <sup>102</sup>J. Brackbill, D. Kothe, and C. Zemach, "A continuum method for modeling surface tension," *J. Comput. Phys.* **100**, 335 (1992).
- <sup>103</sup>R. Issa, "Solution of the implicitly discretised fluid flow equations by operator-splitting," *J. Comput. Phys.* **62**, 40 (1986).
- <sup>104</sup>A. Hager, "CFD-DEM on multiple scales—An extensive investigation of particle-fluid interactions," Ph.D. thesis (2014).
- <sup>105</sup>A. A. Shirgaonkar, M. A. MacIver, and N. A. Patankar, "A new mathematical formulation and fast algorithm for fully resolved simulation of self-propulsion," *J. Comput. Phys.* **228**, 2366 (2009).